The Total Irradiance Monitor Design and On-Orbit Functionality

Greg Kopp, George Lawrence, Gary Rottman
Laboratory for Atmospheric and Space Physics, Univ. of Colorado
1234 Innovation Dr., Boulder, CO 80303

ABSTRACT

The solar Total Irradiance Monitor (TIM) on NASA's SORCE mission began taking data in early 2003. This instrument continues the 25-year record of space-borne, total solar irradiance (TSI) measurements, with improved precision from its new technologies and calibration methods. We present an overview of the TIM instrument, including the design features enabling its high precision, and we present preliminary on-orbit TSI data.

Keywords: total solar irradiance (TSI), SORCE, radiometry, Total Irradiance Monitor, electrical substitution, active cavity

INTRODUCTION

Measurements of total solar irradiance (TSI) are linked to Earth climate and temperature.[1,2] Proxies of the TSI based on sunspot observations, tree ring records, ice cores, and cosmogenic isotopes have given estimates of the solar influence on the Earth that extend back thousands of years, and correlate with major climatic events on the Earth.[3] These estimates extrapolate many recent detailed observations to long-term observations of fewer (or even one) measurement. For example, accurate TSI measurements from the last 25 years are correlated with solar measurements of sunspots and faculae; these correlations can then be used to extrapolate the TSI prior to accurate space-borne measurements, since the solar records extend back 100 years for faculae and 400 years for sunspots. Over this extended time range, the extrapolated TSI record can be compared with longer term records, such as tree rings or ice cores, and correlation with these allows extension of the estimated TSI to more distant times, albeit with decreasing certainty. This extrapolation is important for understanding the relation between TSI and the Earth's climate; yet the extrapolation begins with the comparison of solar surface features to accurate TSI measurements, a record which is currently only 25 years long.

Attempts to measure the TSI began in earnest in the 1830's, with independent measurements by Claude Pouillet and John Herschel, yet were nearly a factor of two low because of atmospheric absorption. Even balloon-borne measurements in the 1900's lacked the instrumental accuracy to detect the ~0.1% changes in the TSI. It was not until long-duration measurements from space were available that changes in TSI were accurately measured and the misconception of a "solar constant" changed. This space-borne TSI record has been uninterrupted since 1978, thanks to overlapping measurements from different missions (see Figure 1). While instrument scale offsets are large, each instrument has high precision and is able to detect small changes in TSI due to variability in the solar surface magnetic features. Increases of 0.1% in TSI during times of solar activity over the 11-year solar cycle are observed, and short-term changes of ~0.3% are attributable to varying sunspot or faculae sizes. However, from the 2 solar cycles observed so far, possible secular changes in the TSI are at low enough level to be difficult to determine.[4] Determination of such long-term solar variability will rely on longer duration measurements of high accuracy, for which continued space-borne TSI measurements are essential.

The SOlar Radiation and Climate Experiment (SORCE) is a Principal Investigator mode NASA mission built and operated by the University of Colorado's Laboratory for Atmospheric and Space Physics (LASP) to monitor both total and spectral solar irradiance for 5 years after its January 2003 launch into a low Earth orbit. The free-flying SORCE includes three instruments measuring spectral irradiance from 0.1 to 3000 nm, and the Total Irradiance Monitor (TIM) to continue space-borne TSI measurements with high accuracy.[5] This paper describes the concept and design of the TIM instrument in more detail than previous publications,[6,7,8] and includes preliminary on-orbit results.
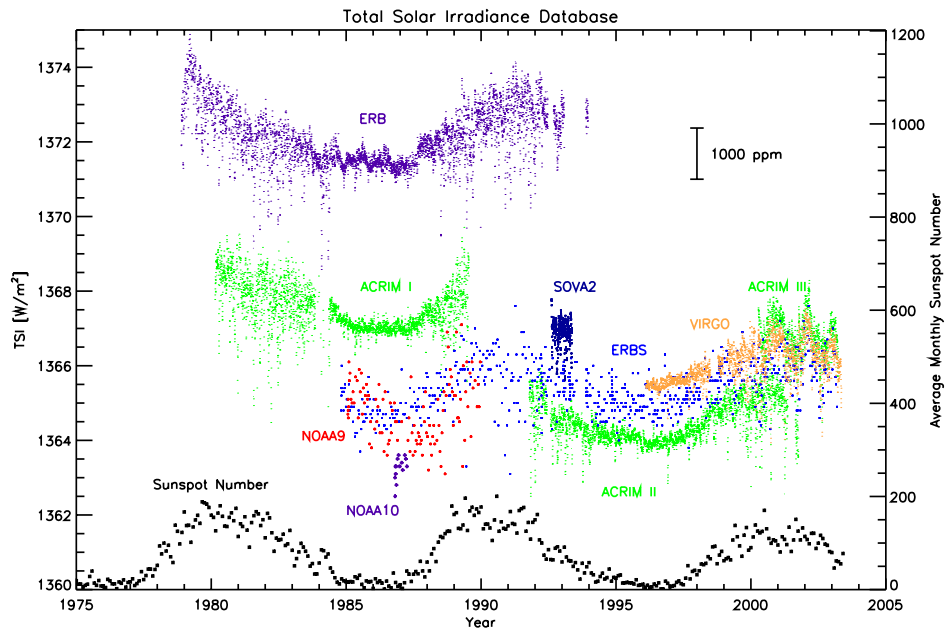
Figure 1: Overlapping measurements from several space-borne TSI-measuring instruments have given an un-interrupted data set since 1978. Note the increase in TSI during times of high solar activity, as indicated by the sunspot record. [ACRIM data are courtesy of Dr. Richard C. Willson, ACRIM Science Computing Facility, Columbia University, 1001 B. Ave. Suite 200, Coronado, CA 92118 via http://www.acrim.com. VIRGO data are courtesy of the VIRGO team, 1997, "In-flight performances of VIRGO solar irradiance instruments on SOHO," Sol. Phys. **175**, pp. 267-286. ERBS data are courtesy of Robert B. Lee III, MS 420, NASA Langley Research Center, Hampton Va. 23681-2199.]

1. TIM DESIGN

The TIM, shown in Figure 2, is an ambient temperature, electrical substitution, null-balance, solar radiometer. The instrument was designed to achieve 10^{-4} relative standard uncertainty in TSI with a precision of 10^{-6}, largely achieved by using phase sensitive detection.[9] Four electrical substitution radiometers (ESRs) provide redundancy and allow degradation tracking via duty cycling. Each ESR has an independent shutter which allows sunlight to enter through a precision aperture to that ESR's absorptive cavity. The electrical power needed to maintain fixed cavity temperature while the shutter cycles, admitting or blocking the incident sunlight, determines the radiative power absorbed by the cavity; this replacement electrical power is the measurement of the entering solar power. The ESRs are pair-wise balanced, one acting as a thermal reference while the other is actively driven to the reference's temperature.

1.1. Phase sensitive detection reduces noise

Phase sensitive detection at the shutter fundamental frequency (10 mHz, 100-s period) reduces sensitivity to thermal drifts, 1/f noise, and parasitic thermal emission from the heat sink (which will be out-of-phase with the shutter). Similar techniques are planned for the upcoming NISTAR radiometer and have been used in an ambient temperature prototype.[10] The shutter frequency was selected near the minimum in the ESR-mounted thermistors' noise power spectrum. The noise density from on-orbit measurements is shown in Figure 3.
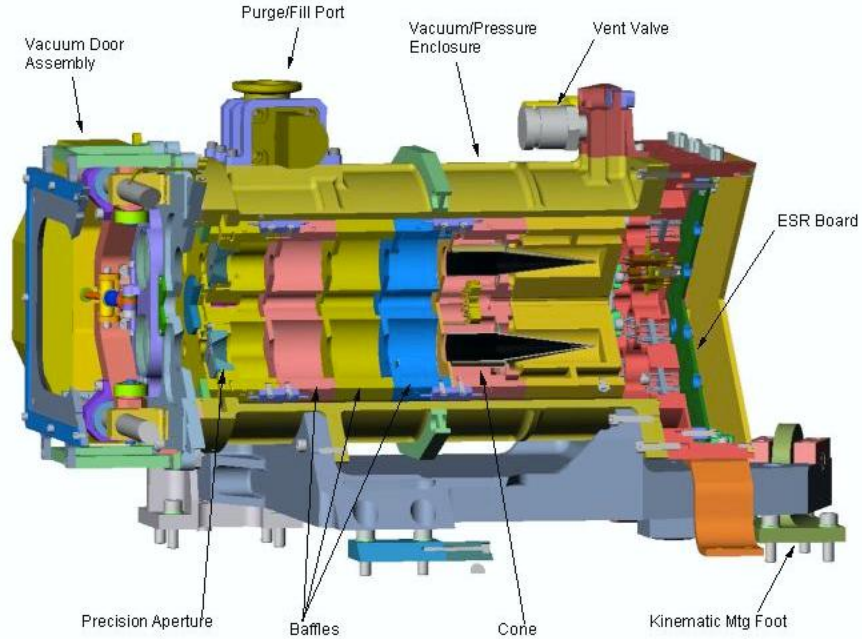
Figure 2: This TIM instrument cutaway shows two of the four absorptive ESR cavities that measure the sunlight modulated by independent shutters. Precision apertures determine the area over which sunlight is collected. Phase sensitive detection at the shutter fundamental reduces noise and determines the total solar irradiance.
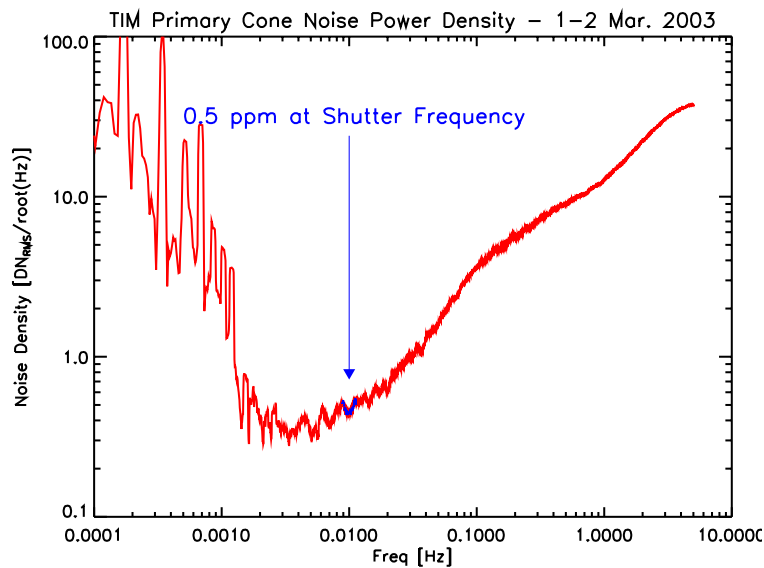

Figure 3: The TIM is operated near the minimum in the noise power density, determined mostly by the ESR thermistors at high frequencies and by orbital variations at low frequencies. At the shutter fundamental, the measured on-orbit noise is less than 2×10^{-6} of the solar signal. A Data Number (DN) is about 21×10^{-6} of the solar signal. The relevant bandwidth to convert power density to fractional solar signal is described in §2.

1.2.   Absorptive cavities have high thermal conductivity

The TIM ESRs are thermally conductive cavities with high absorptivity across the solar spectrum. The high absorptivity helps collect nearly all the entering sunlight, converting it into thermal energy in the cavity. The high thermal

conductivity quickly transports this thermal energy to thermistors that monitor cavity temperature, so that the servo system maintaining the cavity temperature has quick response. High thermal conductivity diamond at the thermal nodes also improves response. A wire-wound resistor embedded in each cavity's outer wall applies heat to nearly the same region of the cavity heated by solar radiation. Closely matching the regions of the cavity heated by the resistor with the region where sunlight is incident reduces the non-equivalence and allows the thermal servo system to operate at higher gain by reducing overshoot. Stainless steel spoked mounts define the predominant thermal path to the TIM's heat sink, which is regulated to maintain a 31°C set point temperature at the cavities. All four cavities are cantilevered from a central hub, reducing the effects of stray thermal gradients. Measured cavity thermal relaxation times are approximately 220 s. Gold plating on the cavity exterior surfaces and on the instrument interior surfaces reduce radiative coupling to the instrument.

The electrodeposited, 15-g ESR cavities are made mostly of silver, providing high thermal conductivity along the 6.3-cm cavity length. At the rear of each cavity is a 4.06 cm long, 10° half-angle cone, which reduces backscatter from spectral reflections and increases the cavity's light absorptivity. A 2.29-cm cylindrical extension at the 1.6-cm diameter mouth reduces the sunlight reflecting out of the cavity. The thermal conduction time from the sunlit rear of the cavity to the thermistors mounted near the cone/cylinder interface is about 2 s.

The cavity interiors are etched nickel phosphorus (NiP), providing cavity reflectances in the range 10^{-4} for solar wavelengths. Being a metal, NiP conducts absorbed radiant power to the cavity well. Tests at the NIST Synchrotron Ultraviolet Radiation Facility indicate low expected degradation of this black absorptive layer to long-term exposure to sunlight.

1.3. Precision apertures define the area over which sunlight is collected

Four diamond turned aluminum apertures, 10.4 cm in front of the cavities, have circular knife edges of diameter 0.8 cm, allowing ≈68 mW of sunlight to enter each cavity. The rather large distance between the aperture and the cavity reduces both input stray radiation and the shutter emission correction, but at the expense of increased loss by diffraction. Black baffles between the apertures and the cavities reduce stray light from the Earth. The flat sunward side of each aperture is highly reflective. The 60° bevel on the rear side is robust during machining and avoids directly incident sunlight from reflecting off the reflective interior aperture surfaces into the instrument. Each aperture is 0.76 cm thick, providing good thermal conductivity to the low-stress mounts to reduce thermal gradients.

1.4. Evanohm wire provides standard resistance

Wound and encapsulated Evanohm wire provides a resistive heater for each cavity; applying a known voltage V across the Evanohm leads heats the cavity with the power V^2/R, where each wire's resistance R is approximately 540 Ω. Evanohm was selected for its low thermal coefficient of resistance, measured at $1.5 \times 10^{-5}/°C$, and for its $<5 \times 10^{-6}$ hysteresis. A doubled strand of polyimide-insulated, resistive Evanohm wire is wound in a spiral groove on the outside of each cavity's conical section, covering the area that is illuminated by sunlight. This winding is epoxy encapsulated under vacuum to maintain good thermal conduction from the winding to the cavity. Overcoatings of chrome and 0.12 mm of copper provide a base for the cavity's outer reflective gold plating, reducing radiative losses. Relative corrections for copper leads in the circuit are about 10^{-4}.

1.5. LTZ1000 provides standard volt

Two Linear Technology LTZ1000 voltage standards provide the reference voltage for each ESR pair. These thermostated, temperature regulated, buried zener diodes supply 7.1 VDC with low thermal sensitivity and low drift. Spreadbury[11] has shown their long-term stability to be better than 3×10^{-6}/yr, and Rax et al.[12] have characterized their radiation stability. This high-precision voltage is digitally pulse-modulated to the cavity heaters via a MOSFET switch having very low (0.004 Ω) turn-on resistance. A set of five such supplies in our laboratory has shown a decrease in voltage of $1 \pm 1 \times 10^{-6}$ /year.

1.6. Fast shutters exceed mission lifetime tests

Each ESR has a separate shutter, located immediately sun-ward of the precision aperture. Each passively bi-stable shutter switches states in 10 ms. The thin aluminum shutters are low mass and mounted with low friction ball bearings. Life tests in thermal vacuum conditions exceed SORCE mission lifetime expectations for the primary cavity's shutter.

Gold plating on each shutter's interior surface reduces thermal emission into the instrument interior, while a thermistor embedded in each shutter allows correction for this thermal emission.

1.7. A DSP controls the TIM's servo systems

A 16 MHz Analog Devices TSC21020F–20MB/833 digital signal processor (DSP) performs all major instrument functions: thermally balancing the ESRs; regulating instrument temperature; maintaining shutter timing; and interfacing commands and telemetry with the spacecraft microprocessor. The DSP operates three 100-Hz AC servo bridges, which thermally balance the two paired ESRs and regulate instrument temperature. The DSP applies power to each cavity at 100 Hz via a field programmable gate array (FPGA) to maintain thermal balance.

A DSP-controlled feedforward allows operation of the servo systems at high gain while preventing servo saturation during shutter transitions, and reduces sensitivity to uncertainty in the servo gain. By anticipating the decrease/increase in electrical power needed to maintain cavity temperature as a shutter opens/closes, the DSP's feedforward reduces the overshoot that would occur if the servo system only reacted to measured changes. The use of feedforward essentially increases the effective servo loop gain and reduces the uncertainty due to measurement of the loop gain.

1.8. TIM instrument peripherals provide diagnostics and corrective capabilities

The TIM ESRs, apertures, and shutters are the core of the instrument. Other items on the instrument help maintain thermal stability, maintain cleanliness, or give diagnostic information. A central heat sink maintains instrument temperature and stability both during a shutter's 100-s cycle period and during the solar-illuminated and eclipsed portions of the 95-min SORCE orbit. A vacuum case with two vacuum doors maintains cleanliness of the instrument interior during integration and launch. Multi-layer aluminized mylar blanketing provides thermal isolation from incident sunlight. Multiple thermistors provide knowledge of various instrument temperatures, and are used in estimating thermal background corrections. Photodiodes monitor the cavity interiors for sudden changes in reflectance, which might be indicative of a change in the absorptive NiP layer. A detector electronics board on the rear of the instrument contains the voltage references in close proximity to the ESRs to reduce the corrections for electrical leads supplying power to the cavity resistive heaters.

2. TIM MEASUREMENT EQUATION

The TIM measurement equation follows from the signal transfer diagram shown in Figure 4. Scalars represent the input irradiance time series E_0, aperture area A, standard voltage V, and standard resistance R, and a time series of output data numbers D. The bold-type terms shown are complex phasor components representing the amplitude and phase of sinusoidal variations as a function of frequency. These complex numbers describe shutter transmission S, thermal impedances Z, and servo gain $-G$ within the instrument. We analyze the TIM at frequencies between 10^{-4} Hz and 50 Hz, but determine the irradiance at the 0.01 Hz shutter fundamental. The data numbers D are output at rates up to 100 Hz, providing a maximum of 10^4 numbers per shutter cycle.
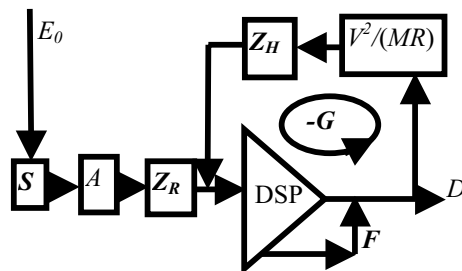

Figure 4: The signal transfer diagram converts input irradiance E_0 to output data numbers D. Bold letters denote complex terms and include a frequency dependence. Shutter S modulates the incoming light entering aperture A. Z_R and Z_H represent the thermal impedances of the cavities to radiative and electrical heat inputs. The DSP adds a known digital feedforward signal F to reduce servo bridge error. We set $|F|$ close to D to make the gain-dependent term in Eqn. 1 small.

In ground data processing, the time series D is frequency analyzed and smoothed using a boxcar filter of the same period as the shutter, which eliminates sensitivity to changes at the shutter frequency. Four successive applications of this filter provide a nearly Gaussian weighting to the data within 200 s of a desired time (see Figure 5). Weighting by sinusoidal components at the shutter frequency produces the complex phasor D which provides knowledge of the changes occurring at and in-phase with the shutter fundamental. This data processing filter has the benefits of Fourier analysis at the shutter frequency while being able to analyze data of only 400-s duration.
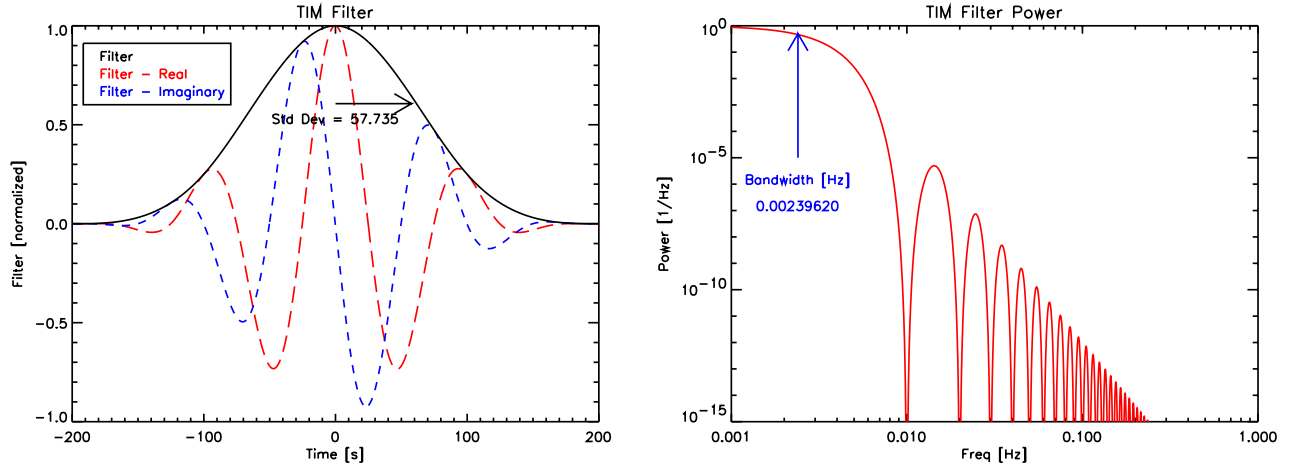

Figure 5: The TIM data processing filter has a total width of 400 s and a standard deviation of 57.7 s in the time response plot shown on the left. The frequency response shown in the plot on the right gives the effective bandwidth as 0.0024 Hz.

The phasors D are converted to measured irradiances via

Eqn. 1
$$E_{\text{meas}} = \frac{V^2}{MR} \cdot \frac{1}{\alpha\,Af} \cdot \text{real}\left\{-\frac{Z_H}{Z_R} \cdot \frac{1}{S} \cdot \left(D + \frac{D-F}{G}\right)\right\},$$

which corrects for the complex servo system gain, shutter timing, equivalence Z_H/Z_R, and applied feedforward values at the shutter frequency, and corrects for the scalar absorptance of the cavity α. Four factors are combined in f to correct for Doppler shifts, the distance to the Sun, cavity sensitivity degradation, and pointing effects. The flight standard voltage V and the standard resistor R determine the standard watt, V^2/R. The fixed scalar $M=64000$ converts data numbers D to duty cycle D/M; the standard voltage is applied to the active cavity's resistive heater at 100 Hz by a modulator applying pulses of width D.

Observations of empty space during the eclipse portion of each orbit provide a measurement of the instrument's thermal signal. These thermal measurements are converted to irradiances, fitted to four instrument temperature measurements as described in §4.2.1, and extrapolated to the daytime side of the orbit to give estimates of the effective thermal signal during solar observations, $E_{\text{dark\_est}}$. The reported TSI value is then the difference

Eqn. 2:
$$E_0(t) = E_{\text{meas}}(t) - E_{\text{dark\_est}}(t)$$

3. RELATIVE STANDARD UNCERTAINTIES

Table 1 summarizes our analyses of the relative standard uncertainty, u. These estimates, described in §4, are assembled from NIST calibrations, analyses, repeatability, and calculations based on parameter uncertainties. The dominant uncertainties are in the aperture A and the cavity absorption α. The individual component uncertainties are assumed independent. Their quadrature sum gives a total standard uncertainty of less than 10^{-4}.

Table 1. Uncertainty budget summary

Factors/corrections	Size $\times 10^6$	$u \times 10^6$
Ephemeris f_{AU}	35000	3
Shutter $\boldsymbol{S}$		3
Aperture A		25
A diffraction	432	52
Reflectance $1-\alpha$	168-360	24-51
Servo Gain, $\boldsymbol{G}$	100	0.1
Standard V^2		10*
Standard R		10
R correct	121	5
Equivalence $\boldsymbol{Z_H}/\boldsymbol{Z_R}$		20
Dark Signal	2000	10
RSS total		68-82

*The voltage uncertainty is likely much higher due to non-linearities discussed in §5.3.

4. TIM CALIBRATIONS

4.1. Ground calibrations

4.1.1. *Cavity absorptance α is high*

We measured cavity reflectance $1-\alpha$ using laser scans of the cavity interiors. A spatial map of cavity reflectance from a 2-dimensional laser scan is averaged over the central region of the cone illuminated by sunlight to obtain an effective reflectance at that laser wavelength. The solar limb-darkened profile is accounted for when computing these averages, although this is a small effect. Seven laser wavelengths (457, 532, 633, 830, 1064, 1523, and 10600 nm) span the primary solar spectrum, with the effective cavity reflectance being the solar-weighted average of the measurements. A spline fit of the reflectance to wavelength interpolates between the discrete laser wavelengths. This fit is constrained at long wavelengths by estimating a reflectance at 100 μm that maintains a smoothly decreasing slope so the fitted long wavelength reflectance never exceeds unity. The effective solar-weighted reflectances for the four TIM cavities are (169, 139, 307, 360) x 10^{-6}. Reflectance uncertainties are 14%, including nearly equal Type B and Type A portions. Measurements of witness cavities using NIST's FTIR[13] indicate the 2 to 20 μm infrared reflectances vary smoothly with wavelength, confirming that we can reliably fit between measured wavelengths.

These ground-based measurements of absorptance are tracked for relative changes on-orbit. Simultaneous, pair-wise intercomparisons of the four cavities used to measure TSI allows monitoring for long-term changes in cavity sensitivity, with the exposure-dependent degradation expected to be lower in the less-used cavities. Additionally, a photodiode monitors the reflected light from each cavity, and is very sensitive to small changes in cavity reflectance.
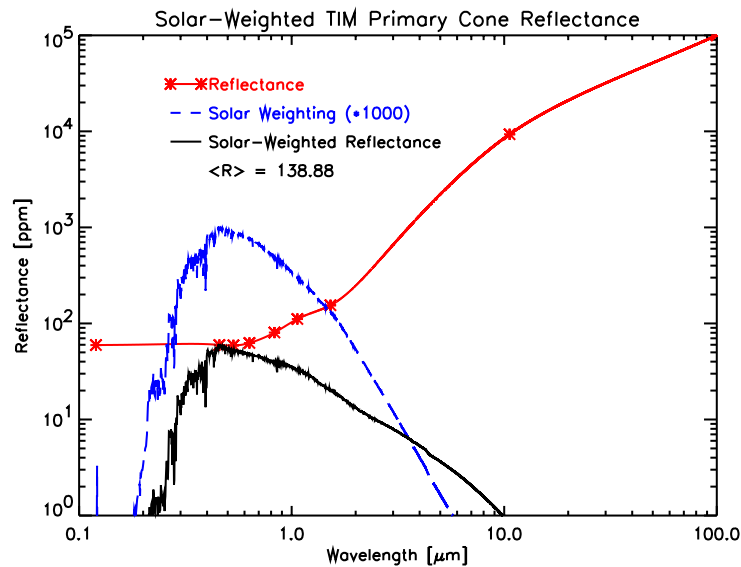
Figure 6: The cavity reflectance increases with wavelength and is smoothly fitted between laser measurements (asterisks). Cavity reflectance is weighted by the relative solar spectral irradiance (dashed line), giving a relative solar-weighted cavity reflectance (solid line); this solar weighting gives the average cavity reflectance, $<R>$.

4.1.2. Aperture area is corrected for diffraction and thermal variations

The areas A of the diamond-turned aluminum apertures were measured at NIST,[14] and are corrected for temperature changes, diffraction, and bulk modulus expansion to the space environment. The four TIM apertures have geometric areas 0.49928, 0.49938, 0.49936, and 0.49926 cm^2 with relative uncertainties of 2.5×10^{-5}. Because of the precision with which NIST can now measure geometric aperture areas, the diffraction correction dominates the TIM aperture area uncertainty. This correction is proportional to the energy-weighted average wavelength $<\lambda>$ of the solar spectrum. Measured solar spectra[15] give $<\lambda>$ = 947 nm, which corresponds to a TIM diffraction correction of 4.3×10^{-4}. Eric Shirley[16,17] of NIST advises that we include 10% (4.3×10^{-5}) of the diffraction correction as uncertainty. We also include corrections for measurements of scattering effects from imperfect edges ($\sim 4 \times 10^{-5}$) and assembly tolerances on alignments. Ground-based measurements of witness aperture areas provide a 2nd order coefficient of thermal expansion appropriate for the apertures' aluminum. A platinum resistive thermal device (RTD) provides the flight apertures' temperature, used in thermal corrections to the area.

4.1.3. Standard watt comes from stable voltage and resistance references

There is no on-orbit monitor of the voltage or resistance references, as no low-mass, space-certified meter with 10^{-6} absolute accuracy is available. The standard watt relies on a 7.1 VDC reference voltage from the temperature-stabilized LTZ1000 diodes applied across resistive windings of encapsulated Evanohm wire, and on pre-flight ground calibrations using a 7.5-digit HP3458A meter under temperature-controlled conditions. Both the standard voltage and the standard resistors were monitored and found stable throughout instrument assembly and spacecraft integration and test, with the final calibrations being three months before launch. Pre-flight measurements of the flight standard voltages have been stable to $<10^{-6}$ in spite of six qualification temperature cycles $-35°C$ to $+50°C$. Qualification temperature cycling of the resistor references have changed their relative resistances less than 3×10^{-6}. Witness LTZ1000 voltage supplies and Evanohm wire continue to be monitored on the ground.

Pre-flight calibrations of the two voltage references give the temperature-corrected voltages
$$V_1 = 7.166434 \, (1. - 0.201404 \times 10^{-6} \, T)$$
$$V_2 = 7.120490 \, (1. - 0.112085 \times 10^{-6} \, T)$$

for temperature T in Celsius. Over three years of continual operation, five laboratory copies of the standard voltage circuits have changed in relative voltage by $-(1\pm1)\times10^{-6}$/year, consistent with previous studies.[11] We will correct at this rate and continue to watch these five, plus eight additional units.

The four Evanohm resistance references are 543.7030, 538.1850, 546.0724, and 537.6500 Ω at the cavity's operating temperature of 30.8°C. Temperature corrections for the Evanohm wire and the electrical leads come from four different instrument temperatures. The measured temperature coefficients of the Evanohm wire itself are near $(8\text{-}10)\times10^{-6}$/°C, close to the specification of the heater wire.

4.1.4. Shutter waveform has small effect on in-phase signal
The shutter moves between a transmission of one when open, and a transmission $<3\times10^{-6}$ when closed. Shutter operation times are 10 ms. With the 100 s shutter period, these times produce a relative correction $<10^{-6}$ in the Fourier transforms of Eqn. 1.

The pre-launch field of view map shows $<10^{-4}$ relative response past 10° off-axis. This rejection suffices to restrict contamination by Earth-shine to < 2.5 minutes around orbital sunrise and sunset. On-orbit pointing performance has not yet been analyzed.

4.1.5. Equivalence
The equivalence ratio $\boldsymbol{Z_H/Z_R}$ in Eqn. 1 comes largely from model calculations and is very near unity with an uncertainty of $<2\times10^{-5}$.[6] This small uncertainty occurs only at the shutter fundamental frequency. The larger non-equivalence at higher harmonics will be used to further constrain the equivalence models. Essentially, the responses at the 3rd and 5th harmonics determine the thermal delay and attenuation of the cavities using the Sun's actual illumination distribution.

4.2. Flight calibrations
4.2.1. Measurements of dark space provide the instrument's thermal background (dark correction)
We measure the instrument's thermal background ("dark") signal by observing space during the eclipsed portion of each orbit. The dark data numbers are converted to irradiances using Eqn. 1, albeit without the Doppler, solar distance, or pointing corrections, which have no relevance for instrument thermal background. These irradiances are fitted to four instrument temperatures, which form the basis vectors for fitting the observed dark irradiances to the linear combination

Eqn. 3
$$D_{\text{Dark}} \approx \sum_{J=1}^{4} C_J T_J^4,$$

where the C_J are determined for best fit and T_J are the four Kelvin temperatures of the cavity, aperture plate, pre-baffle, and shutter. Since the basis vectors in Eqn. 3 are highly correlated, we use the Singular Value Decomposition (SVD) method[18] to isolate individual temperature dependences of the dark signal. The coefficients C_J from the SVD fit have little physical significance and vary sufficiently that the SVD fit is computed every orbit, rather than presuming the C_J remain constant with time. The thermal background during the actual solar observations is then estimated by interpolating this temperature dependence to the daytime portion of the orbit and using temperatures measured during the solar observations.

We measure dark signals of roughly –3.15 W/m². (The negative value is due to the *loss* of energy from the cavities into space when the shutter is opened, so the dark correction in Eqn. 2 increases the measured TSI.) This value varies due to thermal fluctuations in the instrument by 0.1 to 0.2 W/m² between orbital sunset and sunrise. The uncertainty on this dark correction is approximately 0.01 W/m², or less than 10^{-5} of the solar signal.

4.2.2. Gain is monitored on-orbit by analyzing the response to a step function input
The servo gain is calibrated by the DSP bi-weekly to a relative accuracy of 4.5×10^{-4} (see Figure 7). We further set the feedforward value within 1% of the data number, reducing the sensitivity of Eqn. 1 to uncertainty in gain. For TIM gains, with the real part of G$\approx$60, the gain dependent term in Eqn. 1 is thus a $\sim10^{-4}$ relative correction with relative

uncertainty in the final TSI $<10^{-7}$. Additionally, the thermistor bridge resistors are designed so that the gain is at a maximum at the cavity operating temperature, reducing the gain's sensitivity to temperature fluctuations.
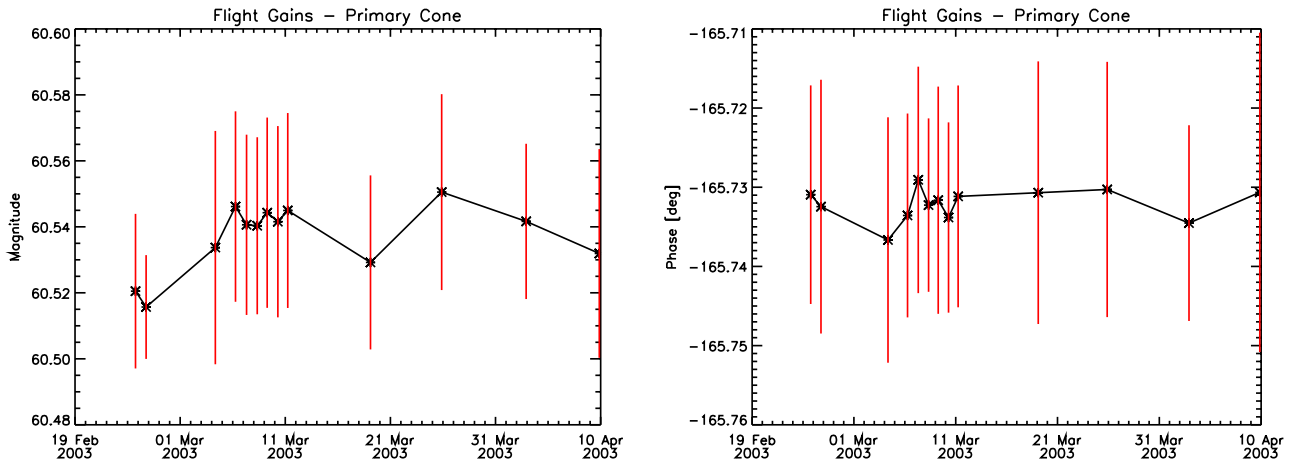

Figure 7: Gain of the primary cavity is measured at least every two weeks by analyzing the response to a DSP-provided step function. The gain magnitude (left) has relative uncertainty 4.5×10^{-4}. Phase (right) is also very constant with time, again having error bars exceeding the variations.

4.2.3. Degradation is monitored via duty cycling cavities and reflectance-tracking photodiodes

To track degradation due to solar exposure, we acquire measurements with the primary cavity nearly all the time, the secondary cavity 1% of the time, the third cavity 0.1% of the time, and the fourth cavity for one orbit annually. Exposure effects can thus be tracked and corrected by a degradation factor that starts at unity at launch. A ground program to monitor unused witness cavities will determine reflectance changes of the cavity NiP due to time alone.

To differentiate between cavity absorptance changes and other system changes, the baffle immediately before the cavities contains four small silicon photodiodes, which continually monitor the reflection from each of the four cavities. Their resolution is better than 0.1% of the reflection; so given a cavity reflectance of 4×10^{-4}, the resolution on relative changes in absorptance is $<4 \times 10^{-7}$.

5. ON-ORBIT OPERATIONS

5.1. Launch and commissioning

The 300-kg SORCE spacecraft was launched by an Orbital Sciences Corporation Pegasus XL into a 600-km, 40° inclination Earth orbit on 25 Jan. 2003. After 5 days of spacecraft commissioning, the instruments were powered on and commissioned, with the 2-day TIM activities starting 6 days after launch. The TIM vacuum doors remained closed for the first two weeks on orbit so that outgassing from the spacecraft could not contaminate the instrument interior. The spacecraft remained pointed 8° off of the Sun for most of the first month on orbit to allow the four SORCE instruments themselves to outgas before illuminating the optics with unfiltered sunlight. Normal data acquisition began on 3 March 2003. All TIM mechanisms and detectors remain fully functional.

During the commissioning period, two wiring errors were discovered:

1) A mis-wiring in each instrument's digital electronics results in an almost daily lock-up during passage through the South Atlantic Anomaly. When locked up, diagnostic telemetry is lost and the instruments will not respond to commands; in the TIM's case, this means that the feedforward value is not updated at Sun/eclipse transitions, causing the servo system to saturate. These data are of no value until the instrument is power cycled, which is now done autonomously by the on-board microprocessor unit after scheduled checks for instrument lock-up on each orbit.

2) The other mis-wiring affects only the TIM, and results in a reduction of gain by a factor of 3.1 in one ESR pair. The other ESR pair is unaffected. Since the DSP implements each ESR's digital proportional-integration-derivative (PID) filter, the gain for this channel has been digitally increased via new PID coefficients.

5.2. Operations

All SORCE operations are commanded from the LASP Mission Operations Center (MOC). The MOC has two contacts per day with SORCE and receives approximately 120 MB/day of telemetry; 10.8 MB is from the TIM. The data are analyzed at LASP. Both raw and analyzed data are stored at the NASA Goddard Earth Sciences' Distributed Active Archive Center (DAAC), where they are available for public use.

From an operations perspective, the TIM is fairly simple. Normal TIM operations are continual measurements of the Sun with the primary ESR cavity during the daytime side of each 95-min orbit, and measurements of dark space during the eclipsed orbit portion. A weekly, 1-orbit, simultaneous primary-to-secondary cavity intercomparison provides degradation knowledge. Approximately every two months, a 1-orbit intercomparison between the primary and tertiary cavities is performed. The secondary cavity is compared with the fourth cavity for one orbit annually. Gain calibration measurements of the primary and secondary cavities are made bi-weekly, and of the remaining two cavities bi-monthly.

A field of view map takes several orbits every 6 months, and provides the TIM sensitivity to pointing that will go into the correction f in Eqn. 1. SORCE solar alignment calibrations that have no TIM relevance cause the loss of about 1 orbit per week of solar viewing.

5.3. Preliminary results

The 6-hourly record of TIM TSI data is shown in Figure 8. These very preliminary data show little degradation with time, even though no degradation correction has yet been applied. On a relative scale, they agree very well with other TSI-monitoring instruments, seeing similar solar features with very low noise. On an absolute scale, however, the data in Figure 8 are approximately 4 W/m^2 lower than the value recorded by other space-borne instruments (see Figure 1). We are currently trying to determine whether this is a calibration or data processing error, or is in fact an accurate measurement. A discrepancy of 4 W/m^2 is 0.3% of the TSI, or about 3 times the stated uncertainty of the non-TIM measurements.
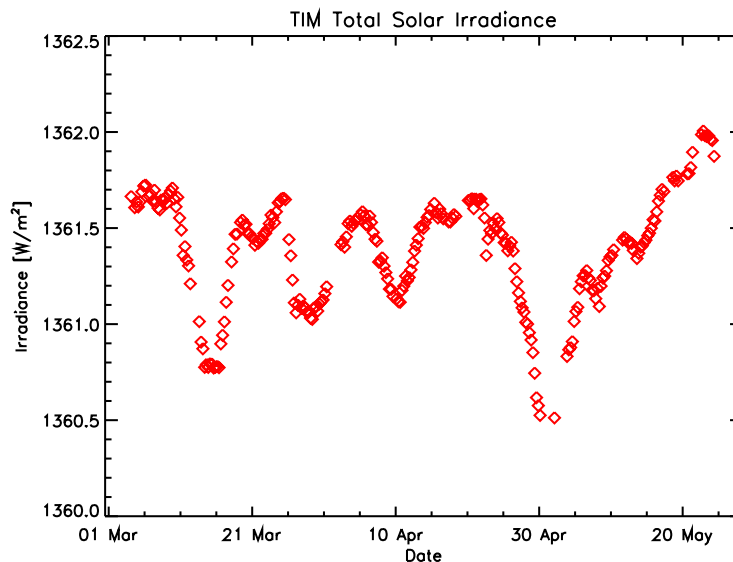

Figure 8: The TIM 6-hourly TSI record shows over the 6-months of observations to date show the passage of several sunspots and sunspot groups (decreases in TSI). These preliminary data have no degradation or pointing corrections applied. The values measured are about 4 W/m^2 lower than other TSI measurements, and calibrations are underway to diagnose this offset.

We have diagnosed a non-linearity in the TIM heater power. Measurements of two flight-similar TIMs are underway and have revealed a linearity correction that needs to be applied to the raw data numbers coming from the flight instrument. This linearity correction improves the agreement between the four TIM cavities, and could potentially give an offset to the absolute value of the TIM TSI.

6. CONCLUSIONS

The SORCE TIM is fully functional and is providing measurements of TSI using a phase sensitive detection scheme. Daily and 6-hourly TSI data are available from the NASA DAAC. The TIM NiP cavities and duty cycling should provide long-term stability of the measured TSI values. Ground linearity calibrations are underway to improve the TIM TSI accuracy.

REFERENCES

1. Foukal, P., "Can Slow Variations in Solar Luminosity Provide Missing Link Between the Sun and Climate?" *EOS*, **84**, #22, 3 June 2003, pp. 205-208.
2. Lean, J., Beer, J., and Bradley, R., "Reconstruction of Solar Irradiance Since 1610:Implications for Climate Change," *Geophys. Res. Lett.*, **22**, 1995, pp. 3195-3198.
3. Pang, K.D. and Yau, K.K., "Ancient Observations Link Changes in Sun's Brightness and Earth's Climate," EOS, **83**, #43, 22 Oct. 2002, pp. 489-490.
4. Willson, R.C. and Mordvinov, A.V., "Secular Total Solar Irradiance Trend During Solar Cycles 21-23," *Geophys. Res. Lett.*, **30**, #5, doi:10.1029/2002GL016038, 2003, p. 1199.
5. Woods, T., Rottman, G., Harder, G., Lawrence, G., McClintock, B., Kopp, G., and Pankratz, C., "Overview of the EOS SORCE Mission," SPIE 4135, 2000, pp. 192-203.
6. Lawrence, G.M., Rottman, G., Harder, J., and Wood, T., "Solar Total Irradiance Monitor (TIM)," *Metrologia* 40, 2000, **37**, pp. 407-410.
7. Lawrence, G.M., Kopp, G., Rottman, G., Harder, J., Woods, T., and Loui, H., "Calibration of the Total Irradiance Monitor," *Metrologia* **40**, 2003, S78-S80.
8. Lawrence, G.M., Rottman, G., Kopp, G., Harder, J., McClintock, W., and Woods, T., "The Total Irradiance Monitor (TIM) for the EOS SORCE Mission," Earth Observing Systems V Proc. SPIE Vol. 4135-21, 2000, pp. 215-224.
9. Gundlach, J.H., Adelberger, E.G., Heckel, B.R., Swanson, H.E. *Phys. Rev. D*, **54**, 1996, R1256-R1259.
10. Rice, J.P., Lorentz, S.R., and Jung, T.M., "The Next Generation of Active Cavity Radiometers for Space-Based Remote Sensing," Preprint volume of the 10th Conference on Atmospheric Radiation, 28 June-2 July 1999, pp. 85-88.
11. Spreadbury, P.J., *IEEE trans. Instrum. Meas.*, **40**, 1991, pp. 343-346.
12. Rax, B.G, Lee, C.I., and Johnston, A.H., *IEEE Trans. Nuclear Science*, **44**, 1997, pp. 1939-1944.
13. Hanssen, Leonard, NIST Optical Technology Division. Private communication, 2002.
14. Fowler, J., Saunders, R., Parr, A., *Metrologia,* **35**, 1998, pp. 497-500.
15. Lean, J., *Geophys. Res. Lett.*, **27**, #16, pp. 2425-2428.
16. Shirley, E., *Applied Optics*, **37**, 1998, 6581-6590.
17. Shirley, E., *NIST Report of Modeling 0000207602*, 2000, 32 pgs.
18. Press, W., Teutolsky, S., Vetterling, W., and Flannery, B., *Numerical Recipes: The Art of Scientific Computing*, Cambridge, 1993.